EUROGRAPHICS 2013 / I. Navazo, P. Poulin
(Guest Editors)

Volume 32 (2013), Number 2

Fleshing: Spine-driven Bending with Local Volume Preservation

Wei Zhuo* and Jarek Rossignac *

* Graphics Visualization and Usability Center, College of Computing, Georgia Tech

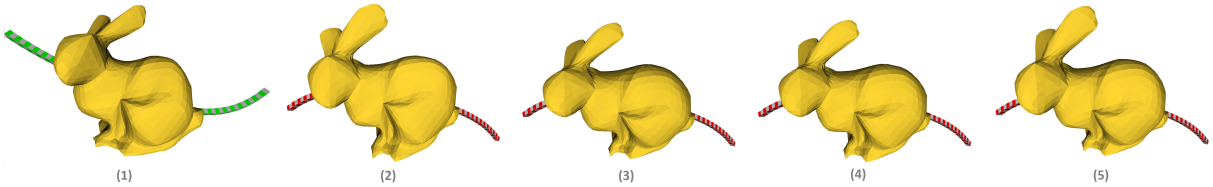

Figure 1: *(1) Original bunny and the initial spine. (2) Result of bending the spine obtained using the standard skinning without volume-preserving correction for which the total volume change is 9%. (3) (4) (5) are the results produced by our three fleshing solutions: radial, normal, and binormal, for which the total volume change (due to sampling and round off errors) is less than 0.3%*

Abstract

Several design and animation techniques use a one-dimensional proxy C (a spine curve in 3D) to control the deformation or behavior of a digital model of a 3D shape S. We propose a modification of these "skinning" techniques that ensures local volume preservation, which is important for the physical plausibility of digital simulations. In the proposed "fleshing" techniques, as input, we consider a smooth spine C_0, a model S_0 of a solid that lies "sufficiently close" to C_0, and a deformed version C_1 of C_0 that is "not overly bent". (We provide a precise characterization of these restrictions.) As output, we produce a bijective mapping M, that maps any point X of S onto a point $M(X)$ of $M(S)$. M satisfies two properties: (1) The closest projection of X on C_0 and of $M(X)$ on C_1 have the same arc length parameter. (2) U and $M(U)$ have the same volume, where U is any subset of S. We provide three different closed form expressions for radial, normal and binormal fleshing and discuss the details of their practical real-time implementation.

Categories and Subject Descriptors (according to ACM CCS): I.3.5 [Computer Graphics]: Computational Geometry and Object Modeling—Geometric transformations F.2.2 [Theory of Computation]: Nonnumerical Algorithms and Problems—Geometrical problems and computations

1. Introduction

Often, the design of a three-dimensional model or of its animation involves bending elongated parts. Models of humans and of various animals are often defined in terms of an articulated skeleton with a few rigid bones connected at (possibly spherical) joints. As the joint angles change, points on the surface or inside the model are moved so as to preserve their relative position with respect to nearby bones. Such "skinning" techniques typically use the arc-length of the closest projection onto individual bones to define relative coordinates and track bone twists (around the bone axis) to fully define the new location of a point after skeletal bending. Points close to a joint may project on more than one bone. The displacements suggested by these different bones are often blended using linear combinations of locations or weighted combinations of rigid motions [LCF00].

Successful techniques have been proposed to increase physical realism of the skin deformations near the joints, so as to more accurately reflect the behavior of skin during the bending of a human elbow [KCZO07]. Some strive to preserve the total volume of the solid near the joint. Other strive to preserve the volume of each slice by possibly tilting the cross-sections [RHC08].

We focus here on deformations that follow the gentle three-dimensional bending of a "spine" that is a smooth curve. Such a tool seems appropriate for bending models of tubes, hoses, wires, ducts, and for approximating the spinal bending of vertebrates (reptiles, fish), and the bending of muscles with no skeletal support, such as mammalian tongues, elephant trumps, octopus arms, or nautilus tentacles. Although such "spine-driven bending" may not be sufficient to model exactly the physically correct behavior of these vertebrae and muscles, it provides an important tool that facilitates the design of useful approximations of their behavior and may have computational advantages over more expensive finite element simulations.

Our main contribution is to propose an explicit mathematical model of spine-driven bending that preserves local volume exactly. By "local" we mean that any solid portion of the initial shape preserves its volume during bending. This objective is more challenging than the preservation of the overall volume (which may for example be achieved by a global scaling or constant distance offsetting [ZR12]) and the preservation of the overall volume of each arbitrary cross-sectional slice using an extension of the Cavalier's Principle [HS97]. Unfortunately, such global or per-slice volume preservation approaches do not provide a volume preserving mapping (homeomorphism) from the initial shape to the final shape. Hence, in these prior approaches, either it is not clear where exactly in a slice a particular chunk of muscle of the initial shape will end up in the bent model, or, when an exact mapping is defined, the volume of the chunk is not preserved.

When the shape is planar and the bending is in that plane, the 2D problem amounts to preserving the local area. An exact solution to local area preserving bending in 2D has been proposed in [ZR12]. It is based on a local correction, which, after the standard bending, adjusts the normal offset (from the spine) of a point based on the curvatures of the initial and the bent versions of the spine at the corresponding (closest projection) point. Our contribution is to extend this prior 2D solution to 3D, where the spine is a possibly non-planar curve and where the goal is to preserve the local volume instead of the area. The extension to 3D is far from trivial. As illustrated in Fig. 2, the solution proposed in [ZR12] is only valid for a point X_0 that lies in the osculating plane of the closest projection Q_0 of X_0 on the initial spine C_0. The solution proposed here does not have this limitation.

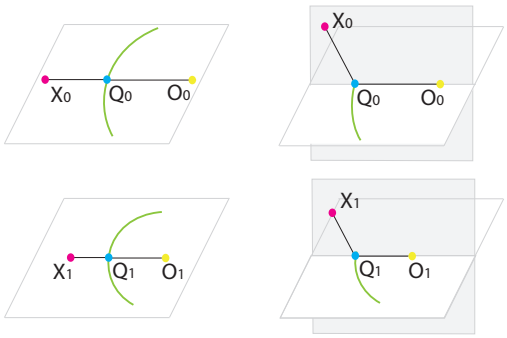

Figure 2: *On the left, we show the planar bending proposed in [ZR12] where Q_0 is the closest projection of X_0 onto spine C_0, O_i is the curvature center of C_i at Q_i. X_i is restricted to lie on the line passing O_i and Q_i. On the right, we show the 3D version of this problem, where X_0 is no longer restricted to lie on the line through O_0 and Q_0. It can be anywhere on the cross-sectional plane orthogonal to C_0 at Q_0.*

1.1. Problem statement and our solutions

The designer starts with a shape S_0 in 3D. Our solution is a mapping from a subset of three-space to another and, as such, it operates on any shape (point cloud, bundle of curves, surfaces, solids, meshes, or cell complexes). Still, because our focus is on volume preservation, for clarity, we say that S_0 is a solid.

The designer first specifies an initial spine C_0. The spine is a smooth curve in 3D that may pierce the solid S_0 or not. In fact, an important benefit of our solution is that the spine may be positioned fully outside of the initial solid. Then the designer specifies a new ("bent") version C_1 of the spine.

We restrict our attentions to formulations that are defined by a mapping M which maps each point X_0 of S_0 to its image $X_1 = M(X_0)$ in S_1. We say that M is a "fleshing" if it satisfies the following conditions:

1. M is fully defined by C_0 and C_1, and hence independent of S_0. This is essential in applications where different versions of S_0 may be used with different resolutions or levels of detail.
2. M is an homeomorphism between S_0 and S_1. This is important because we want the mapping to be invertible: $M^{-1}(X_1) = X_0$, where M^{-1} is defined by the initial spine as C_1 and the final spine as C_0.
3. M maps C_0 to C_1 (i.e., $M(C_0) = C_1$). Because the spines can be adjusted precisely by the user, a solution that ignores such a constraint may be surprising and unnatural.
4. M preserves the arc length along the spine of the closest projection (i.e., $s_0 = s_1$, where s_i $(i = 0, 1)$ is the arc-length parameter of the closest projection of P_i onto curve C_i.) This constraint restricts the mapping to respect cross-sections. Although this constraint seems natural, it may

not be physically correct for some materials that are capable of stretching along the spine [ACWK04]. Nevertheless, this constraint is key to the effectiveness of our solution and a proper assumption if the spine is rigid (only capable of bending and twisting, but not stretching).

5. M preserves volume locally (i.e., $vol(U) = vol(M(U))$ for any subset U of S_0). This is important for the physical plausibility of digital simulations, especially when they involve interactions between evolving solids (swimming creature) and surrounding, incompressible fluids.

1.2. Contributions

We propose three different fleshings that satisfy all of the constraints defined in the previous subsection. We call them "radial", "normal", and "bi-normal". We provide the explicit and mathematically exact expression for each one of these fleshings and explain its derivation.

During interactive manipulation or animation, these fleshings may be computed in real time, at each frame, and animated as the user manipulates the spines. Hence, we advocate their use for gaming and medical simulations where live animation of bending shapes are desired.

Our three solutions produce results that are qualitatively different. To clearly illustrate these differences and help the reader decide which one is appropriate for a particular application, we show in Fig. 4 and 5 comparisons of their effects when S_0 is a tube or extruded cross-section around C_0. We also show in Fig. 1, 7, 6 and 8 their effect on a solid bounded by an arbitrary triangle or quad meshes. We require that C_0 and C_1 be smooth. We provide, for each fleshing, the precise formulation of a valid space in which S_0 must be contained for M to exist as a valid fleshing.

2. Prior Art

The basic deformation operations proposed by Barr [Bar84] extend the conventional operations of affine transformation and CSG to include planar curve-based bending, which preserves the normal offset distance from the spine curve. The resulting mapping is not locally volume preserving as there are local expansion on the convex side and contraction on the concave side of the bent spine. To address this shortcoming, Chrikjian [Chi95] presents a mathematically precise, closed-form solution: for locally area preserving bending in 2D, the offset distance is computed as a root of a quadratic equation with curvature-based coefficients. This variable offset distance allows the shape in the concave side of the spine to grow in the normal direction in order to compensate for the area loss. Moon [Moo08] derives the same quadratic formula for milling with constant material removal rate.

In character animation, Lewis et al. [LCF00] propose generalized forms of skeleton-driven deformations as scattered interpolations. Kavan and colleagues [KCZO07] present the dual quaternion blending as an effective approach to preserve the skinning mesh's rigidity and roughly its local volume around the joint. Constant volume deformations may be defined by a divergence-free vector field as proposed by von Funck et al. [vFTS06]. Angelidis and Singh [AS07] present the computation of divergence-free vector fields induced by skeletal motion. Their framework requires time integration as physically based rigging [CBC*07] and may have computational disadvantages for high resolution meshes. Rohmer and colleagues [RHC08] compute the offset distance scaled by the skinning weight based on affinity and bone-length. To avoid self-intersection, they detect if an offset point is within its region determined by automatic segmentation. Their subsequent work [RHC09] allows the user to specify the locality of the compensation through 1D profile curves that represent isotropic inflation, bulging, or rippling effects.

A classic theorem due to Steiner [Ste40] establishes the relationship between the differential properties of the surface and the volume enclosed. Thus, if we wish to preserve the total volume, we can grow or shrink the shape uniformly (via constant distance normal offsetting rather than global scaling) in one step (without iteration) [ZR12]. Note that this approach minimizes Hausdorff error and may hence be preferred over global rescaling [DMSB99]. It provides an more efficient algorithm for preserving the total volume of a solid undergoing free-form deformation [HML99], or for compensating the volume change due to advection [KLL*07]. To preserve the details of a shape during deformation, one may use registration with the extracted skeleton [STG*97], or with a lower level subdivision model or base surface. Botsch and Kobbelt [BK03] propose to keep the displacement volumes locally constant through relaxation during a deformation of the base surface. Moon [Moo09] presents a closed-form solution for the variable offset distance from a surface that preserves the local volume.

3. Preliminaries

3.1. Locally Volume-preserving Mapping

We consider a bijective mapping $M : X_0 \rightarrow X_1$ that maps any point $X_0 = P_0(x_0)$ onto $X_1 = P_1(x_1)$, where P_0 and P_1 are themselves mappings from local parameters x_0 and x_1 onto Cartesian coordinates. (We use P^{-1} to denote the inverse of a mapping P). The local parameters can be the arc length, radial offset distance and the angle between the offset direction and the Frenet normal. The mapping M is volume-preserving (i.e. divergence-free) if the Jacobian determinant, $det(J(M))$, equals 1 [Chi95]. We compute the Jacobian of M by the following equation:

$$J(M) = \frac{\partial X_1}{\partial X_0} = \frac{\partial P_1}{\partial x_1}\frac{\partial x_1}{\partial x_0}\frac{\partial x_0}{\partial P_0}. \quad (1)$$

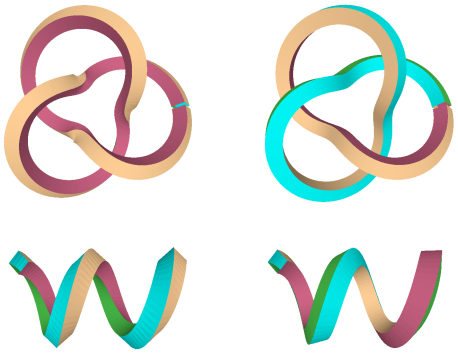

Figure 3: *Left: skinning according to the Frenet frame on a trefoil knot (top) and a helix (bottom). Right: skinning using the normal propagated frame is twist-minimized.*

3.2. Frenet versus twist-compensated local frames

In order to perform skinning, one computes the local frame F_0 of C_0 at the point $C_0(s)$ that is closest to X_0, registers X_0 to F_0, which amounts to computing the local coordinates, and then computes the local frame F_1 of C_1 at the point $C_1(s)$ and constructs X_1 from $C_1(s)$ using the local coordinates. Typically, we select frames that are aligned with the tangent to the spine. Hence, we pick $T_0(s)$ as the tangent to C_0 at $C_0(s)$ and $T_1(s)$ as the tangent of C_1 at $C_1(s)$. The remaining issue is how to determine the other two basis vectors, or their twist around the tangent. A natural candidate for the local frame is the Frenet frame $\{T(s),N(s),B(s)\}$ at $C(s)$ where $N(s)$ and $B(s)$ are the normal and binormal. By Frenet-Serret theorem [dC92], the derivative of the Frenet frame at $C(s)$ is related to the frame itself through the curvature κ and the torsion τ at $C(s)$,

$$\begin{bmatrix} T'(s) \\ N'(s) \\ B'(s) \end{bmatrix} = \begin{bmatrix} 0 & \kappa & 0 \\ -\kappa & 0 & \tau \\ 0 & -\tau & 0 \end{bmatrix} \begin{bmatrix} T(s) \\ N(s) \\ B(s) \end{bmatrix}. \quad (2)$$

Although the Frenet frame provides a convenient local frame along the curve, it is not appropriate as the tool for skinning, because it contains undesired twists, as shown in Fig. 3 (left). For example, the Frenet frame has an orientation discontinuity along a piecewise circular curve [RR87] at the C^1 continuous junction between two adjacent, but not coplanar circular arcs. To address this problem, we use a "twist-compensated local frame", as shown in Fig. 3 (right). Its rotation with respect to the Frenet frame is defined by the integral of the torsion [Sal99] [FH03]. We construct the twist-compensated normal $I(s+ds)$ at $C(s+ds)$ by projecting $I(s)$ to the normal plane of $C(s+ds)$. Therefore, given an initial normal $I(0)$, the twist-compensated normal $I(s)$ is obtained by propagation from $I(0)$. Then for each point X_0 of S_0, we register it with the twist-compensated cross-sectional frame $W_0(s) = \{I_0(s), J_0(s)\}$ on $C_0(s)$.

3.3. Overview of the fleshing algorithm

We are given a solid S_0, an initial spine C_0, and a final spine C_1. We are also given an initial normal vector $I_0(0)$ to C_0 at $C_0(0)$ and an initial normal vector $I_1(0)$ to C_1 at $C_1(0)$. Alternatively, we compute $I_0(0)$ and $I_1(0)$ automatically, using an agreed upon rule for generating a vector normal to a tangent direction, and let the designer control the global twist angle w which we use to adjust $I_1(0)$ by rotating it around the tangent to C_1 at $C_1(0)$. We assume that each point of S_0 has a unique closest projection on C_0 and that C_1 satisfies our validity conditions. We compute the bent version S_1 of S_0 by applying a fleshing to every vertex or control point X_0 of S_0 to obtain its image $X_1 = M(X_0)$. Our approach involves the following steps:

1. *Registration*: For each vertex X_0 of S_0, we compute the arclength parameter s_0 of its closest projection $Q_0 = C_0(s_0)$ and the corresponding Frenet cross-sectional frame $F_0 = \{N_0, B_0\}$ and twist-compensated frame $W_0 = \{I_0, J_0\}$. We compute the local parameters x_0 of X_0 in F_0.
2. *Unbending*: We compute the image x_u of x_0 produced by a local volume preserving unbending.
3. *Transfer*: We compute the parameters of x_u in W_0, compute the corresponding twist compensated frame W_1 at s_0 on C_1, use these parameters in W_1 to produce a point, and compute the parameters x_t of that point in the corresponding cross-sectional Frenet frame F_1 on C_1.
4. *Bending*: We compute the image x_1 of x_t produced by bending a straight line to obtain curvature κ_1 of C_1 at $Q_1 = C_1(s_0)$. Then we use the parameters x_1 in F_1 to construct the image $X_1 = M(X_0)$.

In Sec. 4, we provide three versions of unbending $x_u = unbend(x_0, \kappa_0)$ and of bending $x_1 = bend(x_t, \kappa_1)$.

3.4. Validity conditions

To express the validity conditions under which our approach produces a fleshing, we define a valid space $S(C_0, C_1)$ which must contain S_0. To do so, we define the "reach" $R(C)$ of a curve C as the locus of all points that have a unique normal projection onto that curve. The reach may be computed as the space obtained by radially inflating the curve at each point and in all orthogonal directions until we reach the corresponding curvature axis (which is the axis of the osculating circle). We define $S(C_0, C_1)$ as the intersection $R(C_0) \cap M^{-1}(R(C_1))$ of the reach of C_0 with the pre-image of the reach of C_1. In Sec. 4, we provide explicit formulae for testing, during unbending and bending whether a point X_0, is in the valid space.

4. Fleshings

We present three fleshings: radial, normal and binormal. For each, we discuss a general derivation satisfying $det(J(M)) = 1$, and special cases for unbending and bending.

4.1. Radial Fleshing

Radial fleshing is denoted by M_r. We start with the point X parameterized by (s,r,θ). s is the arc length parameter of the closest projection $C(s)$ of X onto C. r and θ are the polar coordinates of X on the normal plane of $C(s)$:

$$X = P(s,r,\theta) = C(s) + r\cos\theta N(s) + r\sin\theta B(s).$$

We take the derivative of X with respect to its parameters and substitute T', N' and B' by using Frenet-Serret equation (Eq. 2), and reduce the result to

$$\frac{\partial X}{\partial(s,r,\theta)} = \begin{bmatrix} (1-\kappa r\cos\theta) & -\tau r\sin\theta & \tau r\cos\theta \\ 0 & \cos\theta & \sin\theta \\ 0 & -r\sin\theta & r\cos\theta \end{bmatrix} \begin{bmatrix} T(s) \\ N(s) \\ B(s) \end{bmatrix}. \quad (3)$$

Therefore, we have:

$$det(\frac{\partial X}{\partial(s,r,\theta)}) = r(1-\kappa r\cos\theta). \quad (4)$$

In $M_r : X_0 \to X_1$, we assume that only the radial offset distance r is updated from r_0 to r_1 while other parameters remain the same. We solve for r_1 under the constraint that $det(J(M_r)) = 1$. We next show that there exists an closed-form solution for r_1, and hence an analytic solution for M_r. Specifically, from Eq. 1 we have:

$$J(M_r) = \frac{\partial X_1}{\partial(s,r_1,\theta_1)} \frac{\partial(s,r_1,\theta_1)}{\partial(s,r_0,\theta_0)} (\frac{\partial X_0}{\partial(s,r_0,\theta_0)})^{-1}. \quad (5)$$

Given Eq. 4, we compute the determinant of the Jacobian in Eq. 5 as:

$$\begin{aligned} det(J(M_r)) &= det(\frac{\partial X_1}{\partial(s,r_1,\theta_1)}) \frac{dr_1}{dr_0} / det(\frac{\partial X_0}{\partial(s,r_0,\theta_0)}) \\ &= \frac{r_1(1-\kappa_1 r_1\cos\theta_1)}{r_0(1-\kappa_0 r_0\cos\theta_0)} \frac{dr_1}{dr_0}. \end{aligned}$$

In order to let $det(J(M_r)) = 1$, we solve the following ODE:

$$r_1 dr_1 - \kappa_1 r_1^2 dr_1\cos\theta_1 = r_0 dr_0 - \kappa_0 r_0^2 dr_0\cos\theta_0,$$

and integrate from 0 to r_i on both sides of the above equation to obtain:

$$-\frac{2}{3}\kappa_1\cos\theta_1 r_1^3 + r_1^2 = -\frac{2}{3}\kappa_0\cos\theta_0 r_0^3 + r_0^2. \quad (6)$$

Therefore, r_1 is a cubic root of Eq. 6 with coefficients specified by r, κ_0, κ_1 and $\cos\theta$. The solution provided by Eq. 6 assumes that the bending (change of curvature) does not change the local Frenet frame. To support more general bending, as explained in Sec. 3.3, we split the fleshing into several steps which include *unbending* (locally at $C_0(s)$, the spine becomes a straight line) and *bending* (the spine becomes curved again with the new curvature and normal). Here, we provide the formulae for the unbending and bending steps.

Radial Unbending: We first assume that $C_0(s)$ is straightened into a line (i.e. $\kappa_1 = 0$) and solve for a temporary value r_*:

$$r_* = r_0\sqrt{1 - \frac{2}{3}\kappa_0\cos\theta_0 r_0}. \quad (7)$$

In order for r_* to exist, $\frac{2}{3}\kappa_0\cos\theta r_0 < 1$. As $\cos\theta$ varies in $[-1,1]$, an sufficient condition for r_* to exist is $|\kappa_0 r_0| \le \frac{3}{2}$.

Radial Bending: We then bend the straight spine into C_1 and solve for r_1 using r_*:

$$-\frac{2}{3}\kappa_1\cos\theta_1 r_1^3 + r_1^2 = r_*^2. \quad (8)$$

We normalize the unknown and the coefficients in Eq. 8. Specifically, let $\lambda = \frac{r_1}{r_*}$ and $\alpha = -\frac{2}{3}k_1 r_*\cos\theta$, then Eq. 8 becomes $\alpha\lambda^3 + \lambda^2 = 1$. Let $f(\lambda) = \alpha\lambda^3 + \lambda^2 - 1$, which has two local extrema (minimum at $\lambda_1 = 1$ and maximum at $\lambda_2 = -\frac{2}{3\alpha}$). If $\alpha > 0, \lambda_2 < 0$, then $f(0)f(1) < 0$ and $f' > 0 \in [0,1]$, and hence there exists a valid solution in $[0,1]$. If $\alpha > 0, \lambda_2 > 0$, then a valid solution exists only if $f(\lambda_2) > 0$, or equivalently $\alpha^2 < \frac{4}{27}$. Again since $\cos\theta$ varies in $[-1,1]$, an sufficient condition for r_1 to exist is $|\alpha| < \frac{2}{3\sqrt{3}}$, or

$$|\kappa_1 r_*| \le \frac{1}{\sqrt{3}}, \quad (9)$$

and when κ_1 reaches this curvature limit, $r_1 = \sqrt{3}r_*$.

Fig. 4 illustrates the bending of a straight spine into a circular arc. Fig. 4 (a) is the original spine with two layers of cylindrical tube surfaces. Fig. 4 (b) shows the application of Radial Bend to the original tube. Intuitively, the radial distance increases for points on the inner side of the curved spine in order to compensate for local compression. Excessive bending over the curvature limit in Eq. 9 leads to self-intersection of the tube surface.

4.2. Normal Fleshing

Here, we define the normal fleshing M_n. We consider expressing a point X in the local Frenet frame as follows:

$$X = P(s,x,y) = C(s) + xN(s) + yB(s).$$

We take the derivative of P with respect to its parameters and substitute the derivatives using Eq.2:

$$\frac{\partial X}{\partial(s,x,y)} = \begin{bmatrix} (1-\kappa x) & -\tau y & \tau x \\ 0 & 1 & 0 \\ 0 & 0 & 1 \end{bmatrix} \begin{bmatrix} T(s) \\ N(s) \\ B(s) \end{bmatrix}.$$

Therefore,

$$det(\frac{\partial X}{\partial(s,x,y)}) = 1 - \kappa x.$$

During normal fleshing, we change the parameter x from x_0 to x_1 while keeping s and y constant. Given κ_0, κ_1, s, y

and x_0, we solve for x_1 under the constraint $det(J(M_n)) = 1$. Specifically, we have:

$$\begin{aligned} det(J(M_n)) &= det(\frac{\partial P_1}{\partial(s,x_1,y)})\frac{dx_1}{dx_0}/det(\frac{\partial P_0}{\partial(s,x_0,y)}) \\ &= \frac{(1-\kappa_1 x_1)dx_1}{(1-\kappa_0 x_0)dx_0}. \end{aligned}$$

Setting $det(J(M_n)) = 1$ gives that:

$$dx_1 - \kappa x_1 dx_1 = dx_0 - \kappa_0 x_0 dx_0.$$

Integrate on both sides of the above equation and we have:

$$x_1 - \frac{1}{2}\kappa_1 x_1^2 = x_0 - \frac{1}{2}\kappa x_0^2. \tag{10}$$

Therefore, x_1 is a quadratic root of Eq. 10 with coefficients specified by x_0, κ_0, κ_1.

As for Normal Fleshing, Eq. 10 is limited to cases where the local curvature is changed, but the Frenet frame remains constant. To support more general fleshing, as explained in Sec. 4.1, we provide below its decomposition into normal unbending and bending maps, which may be combined with the twist-compensated rotation, as discussed in Sec. 3.3. To solve x_1, we break Eq. 10 into two steps:

Normal Unbending: Assume that $C_0(s)$ is first straightened ($\kappa_1 = 0$) and we solve for a temporary value x_*,

$$x_* = x_0(1 - \frac{1}{2}\kappa_0 x_0). \tag{11}$$

As $\frac{x_*}{x_0} \geq 0$, the condition for a valid solution of r_* to exist is $|\kappa_0 x_0| \leq 2$.

Normal Bending: We then bend the straight spine into C_1 and solve for x_1 using x_*:

$$-\frac{1}{2}\kappa_1 x_1^2 + x_1 = x_*. \tag{12}$$

Hence, the closed-form solution for x_1 is

$$x_1 = \frac{1 - \sqrt{1 - 2\kappa_1 x_*}}{\kappa_1}.$$

In order for x_1 to be valid, we have:

$$\kappa_1 x_* \leq \frac{1}{2}, \tag{13}$$

and when κ_1 reaches this curvature limit, $x_1 = 2x_*$.

Fig. 4 (c) shows the application of Normal Bending to the cylindrical tube surfaces in Fig. 4 (a). As shown in the cross-sectional plot, M_n slides points in the normal direction. Intuitively, the tube surface stretches towards the inner side and shrinks from the outer side of the circular spine in order to compensate for local compression and expansion. When reaching the curvature limit in Eq. 13, the tube surface starts to intersect itself. Note that M_n has a more stringent curvature limit than M_r for the same initial tube surface.

4.3. Binormal Fleshing

During the Binormal Fleshing, we adjust the coordinate from y_0 to y_1 while keeping s and x constant. We then solve for y_1 under the constraint $det(J(M_b)) = 1$:

$$det(J(M_b)) = \frac{(1-\kappa_1 x)dy_1}{(1-\kappa_0 x)dy_0}.$$

We set $det(J(M_b)) = 1$ to obtain,

$$(1-\kappa_1 x)dy_1 = (1-\kappa_0 x)dy_0.$$

Therefore,

$$(1-\kappa_1 x)y_1 = (1-\kappa_0 x)y_0. \tag{14}$$

This result shows that y_1 is linearly related to y_0 with the coefficient defined by κ_0, κ_1 and x.

Binormal Unbending: Let $\kappa_1 = 0$, $y_* = y_1$ and we have,

$$y_* = (1-\kappa_0 x)y_0. \tag{15}$$

In order for y_* to be valid, we have $\kappa_0 x \leq 1$.

Binormal Bending: Let $\kappa_0 = 0$, $y_0 = y_*$ and we have,

$$y_1 = \frac{1}{1-\kappa_1 x}y_*. \tag{16}$$

In order for y_1 to be valid, we have

$$\kappa_1 x < 1. \tag{17}$$

When κ_1 reaches this curvature limit, y_1 becomes unbounded.

Fig. 4 (d) shows the application of Binormal Bending to the cylindrical tube surfaces in Fig. 4 (a). As shown in the cross-sectional plot, M_B only allows stratification in the binormal direction: points on the tube surface expand or shrink bilaterally on the inner side or the outer side of the circular spine. When reaching the curvature limit in Eq. 17, the tube surface becomes flat on the inner side. Note that M_b has the least stringent curvature limit among the three solutions.

Discussion: Note that Eq. 6, Eq. 10 and Eq. 14 are symmetric in the initial and final states of the spine and the space point. Hence, the mappings are homeomorphisms between S_0 and S_1. Fig. 4 presents a qualitative comparison of the three fleshing solutions by showing their effects on tubular surfaces: Bi-normal fleshing is closest to what happens when a tube is bent horizontally a bit too much: the flesh is pushed vertically up or down (as in the crack of a bent elbow). The normal fleshing is the reverse: the flesh moves horizontally, hence it moves more quickly in the direction of the center of curvature. The radial is a compromise, the flesh moves radially away or towards the spine.

5. Experiments and Results

This section shows the results of our three fleshing solutions.

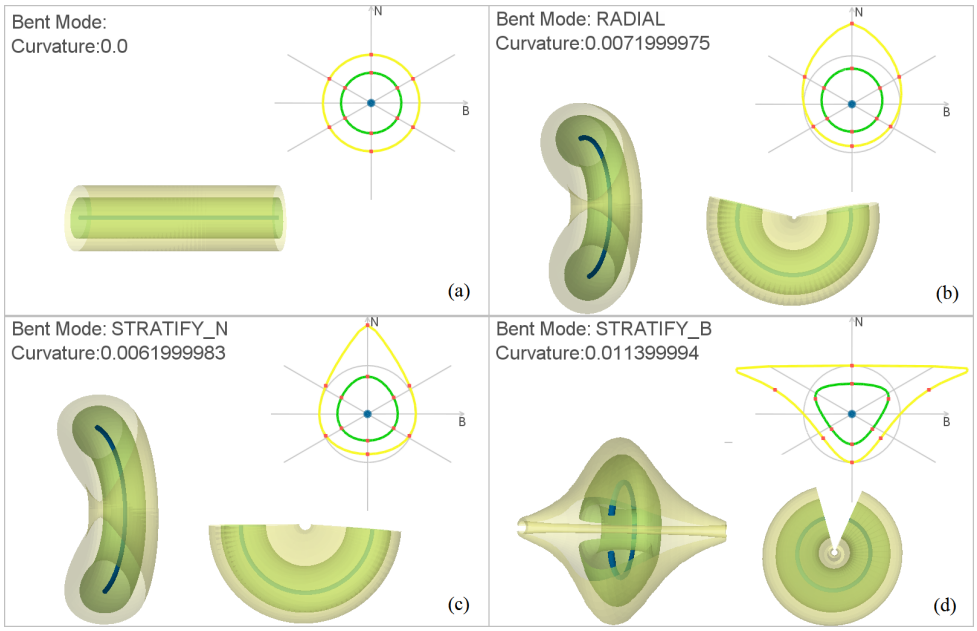

Figure 4: *The deformation of two layers of tube surfaces driven by bending a straight spine into a circular arc. We show three types of fleshing to the original tube surfaces. Each shows the transverse (left) and the frontal (right) views of the bent tubes, and the cross section is dynamically plotted on the top-right. The red marks show the selected mapping of points.*

5.1. Extrusion Models

We first present the application of fleshing to models of solids produced by sweeping a user specified planar cross-section along a smooth 3D spine curve. To better show the different effects of our three solutions, we apply them to extrusions along spines that are circular arcs. In the 2D view as shown in Fig. 5, the user draws a contour and indicates the point $Q = Q_0 = Q_1$ at which the initial and the final spines are aligned and have the same tangent, but different radii and osculating planes. The centers of the arcs are specified by locations O_0 and O_1. We show the initial cross-section in blue, then for each fleshing, we show the result of unbending in green and in red the result of bending the green in Fig. 5(b). The vectors O_0Q and O_1Q define the Frenet frames and curvatures. We assume here no twist (i.e., $\theta_1 = \theta_0$). Notice that the radial fleshing nearly preserves straight lines (even though it is not an affine map). In Fig. 5(c), we show the results in 3D and the corresponding statistics in Tab. 1.

We compute the exact volumes of the extrusion models in all cases using the following approach. Let W be the centroid of a planar region R and let Q be the point passed by the arc C with length l and center O. Then the volume of the solid S swept out by R along C is computed as [Foo06],

$$vol(S) = area(R)\rho l$$

where $\rho = \frac{OW \cdot OQ}{|OQ|^2}$ is the ratio of the actual distance traveled by the centroid and l. If C is a line, $\rho = 1$. We compute the relative error ε of the solid S as

$$\varepsilon = \frac{vol(S_1) - vol(S_0)}{vol(S_0)}$$

where S_i is the solid swept out by R_i along C_i, $i = 0, 1$. As shown in Tab. 1, models without fleshing have relatively large volumetric errors (3%-5%). The other 6 models with fleshing have nearly the same volume with very small (less than 0.03%) volumetric errors.

	$area(R)$	ρ	$vol(S)$	ε
Original	0.278	1.032	1.436	0
Unbend	0.278	1	1.391	-0.031
Bend	0.278	0.982	1.366	-0.049
Radial Unbend	0.287	1	1.436	-1.36E-5
Radial Bend	0.296	0.969	1.436	-3.97E-6
Normal Unbend	0.287	1	1.436	-5.63E-5
Normal Bend	0.298	0.963	1.436	-1.03E-4
Binormal Unbend	0.287	1	1.436	1.17E-4
Binormal Bend	0.293	0.979	1.437	2.83E-4

Table 1: *Statistics of the cross-sectional areas, ratios of the centroid traveled distance to l, solid volumes and their relative errors for extruded models in Fig. 5(c).*

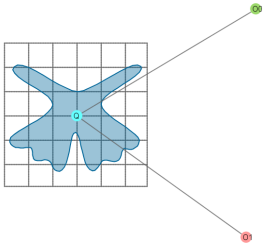

(a) the cross section of the original solid (blue) and the unbending and bending directions specified by Q, O_1, O_2

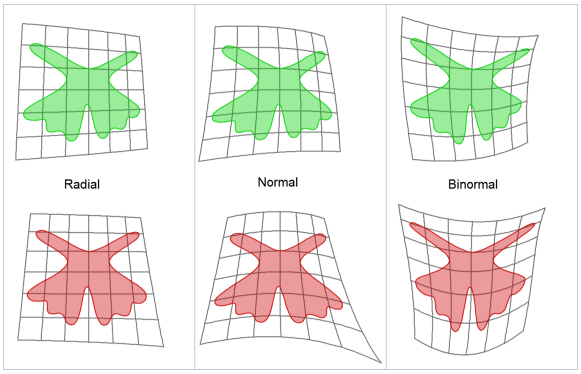

(b) From left to right, we show the radial, normal and binormal fleshings in two steps: the top row is the unbend images and the bottom row is the bend images of the top row.

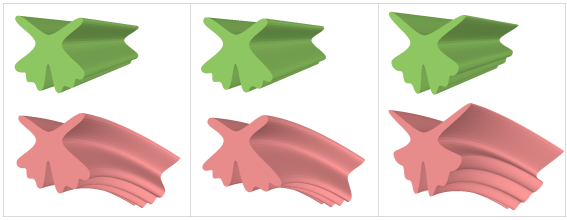

(c) 3D extrusion models correspond to the cross sections in Fig. 5(b)

Figure 5: *Fleshing mappings of a extrusion model*

5.2. Quad and Triangle Meshes

We show fleshing applications to general shapes and report total volume changes of less than 0.3%. Fig. 1 shows bending a triangle mesh representing a bunny.

Fig. 6 shows bending a genus-2 quad mesh first with a vertical spine into the frontal plane, then with a horizontal spine out of the frontal plane. Initially, the red and the blue spines are on the plane that divides S_0 into identical halves. Without the volume-preserving mapping, the volume remain unchanged after the first bending, but increases by 9% after the second bending. In comparision, the volume deviates little (<0.1%) from the orginal one if using fleshing. However, the binormal stretch (Fig. 6(b) right) causes the mesh to grow unexpectedly in the horizontal direction. Fig. 7 shows

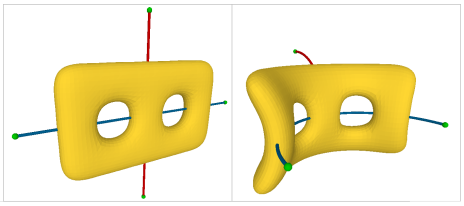

(a) bending a subdivision mesh (the original volume is 2.1530) with two axis-aligned circular arcs. The deformed mesh without fleshing (right) is 2.3493.

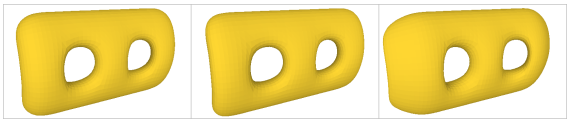

(b) first bend the red arc: the volumes of the M_r, M_n, M_b mapped meshes are 2.1526, 2.1527 and 2.1526 from left to right.

(c) then bend the blue arc: the updated volumes are 2.1516, 2.1522 and 2.1508

Figure 6: *successively bending a mesh*

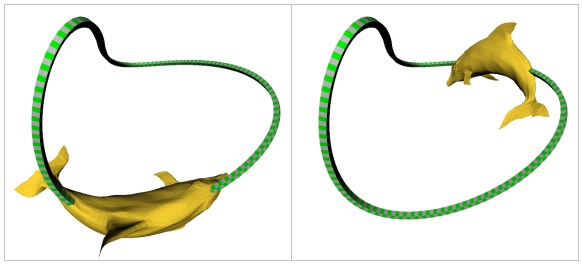

Figure 7: *Two frames in an animation of a dolphin sliding along a 3D curve: by using the radial fleshing, the volume deviations of the mesh model are 0.12% and 0.08% in these two positions. In comparison, the volume deviations are 6.75% and 3.47% without fleshing.*

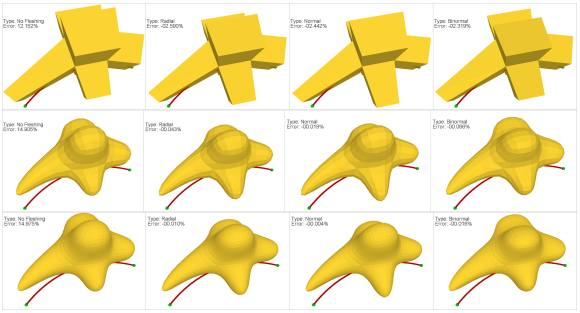

Figure 8: *From left to right we show the bending results of skinning, radial, normal and binormal on different levels of a subdivision mesh. From top to bottom, the number of vertices are 32, 482, 1922.*

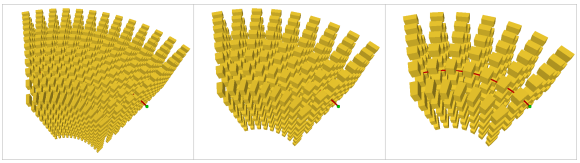

Figure 9: *Bending a cloud of cubes of uniform size. From left to right, the original cube sizes are 15, 22, 30.*

an application in animation, where a dolphin mesh is sliding along a 3D curve (produced by changing the origin of the arc-length for C_1) with its orientation and deformation determined by the curve. Here the curve, C_1, represents a animator-specified path for the digital model to follow. The path may be curved so that the model may bend. Without fleshing, this causes unexpected changes of volume perceivable by the viewer. The volume of the digital model is preserved by one of our fleshing mappings. As shown in the figure, the volume deviation is above 5% without fleshing and reduced to 0.01% with the radial method.

5.3. Resolution and Accuracy

This section discusses the impact of sampling density on the accuracy of (local) volume preservation implemented by fleshing. Fig. 8 shows bending a subdivision mesh at different resolutions. The increase of the subdivision depth greatly decreases the relative volume errors of the three fleshing mappings (from 2.5% to 0.001%). On the contrary for skinning without fleshing, the relative volume error increases slightly (from 12% to 15%). This shows that fleshing mappings give accurate total volume-preserving results for high resolution meshes. In fact, our objective is not only to preserve the total volume, but to preserve the local volume for each small chunk of the solid. Hence, the proper measure of volume error that should be used to demonstrate the benefit

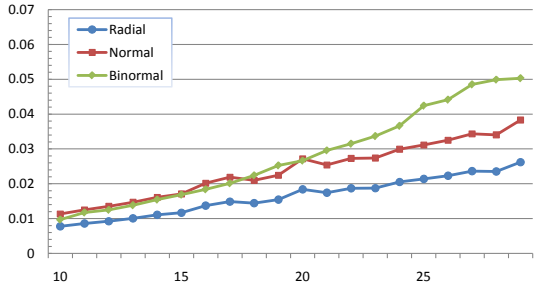

Figure 10: *plot of the percentage mean absolute relative error versus the cube size*

of fleshing over skinning is to report the average of the absolute volume errors of the small chunks. Fig. 9 shows bending a cloud of cubes at different sizes. We compute the volume of each cube deformed by the spine. The relative error for each cube is computed as $\varepsilon = (v - v_0)/v_0$. We report the percentage mean absolute value, ε_{mean}, of the relative errors for all cubes. Fig. 10 shows the plot of ε_{mean} versus the cube size. In general, the relative error scales with the cube size in all three fleshing mappings. The volume error reported for large cubes comes from approximating the curved shape of the bent cube by a polyhedron that interpolates the images of the vertices of the initial cube.

6. Discussion

Fleshing presents three closed-form volume preserving mappings, which depend on a proper local parameterization of the 3D shape along the 1D spine. The spine may have a simple parametric expression, such as circular or helical arc. Then the closed-form parameterization along the curve is easy to obtain. However, this limits the designer's ability to bend the spine by manipulating control points. If we represent the spine by a interpolating polynomial, we must be able to compute the arc-length parameter of the closest projection of a point onto the spine efficiently.

The choice of representation for the spine is orthogonal to our contribution. Nevertheless, we support two formulations for the spine C: (1) a low degree, interpolating polynomial, which we evaluate using Neville's algorithm, as shown in Fig. 1, and (2) quintic NUBS, which we evaluate using de Casteljau's algorithm, as shown in Fig. 7. C_0 and C_1 are polygonal approximations of such smooth curves. We sample them so as to ensure a constant distance, d, between consecutive samples. Again, let Q_0 be the closest projection of X_0 on C_0. Assume that Q_0 is on the edge $C_0[k]C_0[k+1]$:

$$Q_0 = C_0[k] + aC_0[k]C_0[k+1], \quad 0 < a < 1.$$

The arc-length parameter s of Q_0 is $s = (k+a)d$. We use the same arc-length parameter to compute Q_1 on C_1: $Q_1 =$

$C_1[k] + aC_1[k]C_1[k+1]$, which is used as the anchor point for computing X_1, as described in the overall fleshing transformation. The influence of this polyline approximation depends on the sampling step size (d). When d is not overly small, decreasing d improves the precision for locally volume preservation. Angular distortion exists in fleshing mappings due to that the mappings are not conformal. Also, it is not possible to deform B-spline surfaces with locally volume preservation by applying the mapping only to its control points as the mappings are not affine. However, fleshings preserve smoothness, and hence also sharp features. In fact, the radial fleshing is nearly line preserving, as shown in Fig. 5(b) (left). The result is guaranteed to be free from self-crossing (when we are within the validity conditions), and hence it will not produce new sharp features.

7. Conclusion

We have proposed three formulations for deforming a shape driven by bending a spine. Our fleshing solutions ensure that the local volume of any subset of a valid space is preserved during the bending. Furthermore, our solution is based on a closed form mapping of space and depends neither on the initial shape nor on the given global coordinate system. Hence the fleshing may be applied to any shape topology (point cloud, watertight surfaces or cell complexes). Furthermore, we extend our approach to free form spines, by propagating a twist compensated local frame and by letting the user or an application control the bending and twisting. We hope that the simplicity, accuracy and performance of the proposed fleshing approach will make it a standard bending tool for many modeling and animation applications where local volume preservation is desired.

References

[ACWK04] ANGELIDIS A., CANIF M., WYVILL G., KING S.: Swirling-sweepers: constant-volume modeling. In *Computer Graphics and Applications, 2004. PG 2004. Proceedings. 12th Pacific Conference on* (2004), pp. 10 – 15. 3

[AS07] ANGELIDIS A., SINGH K.: Kinodynamic skinning using volume-preserving deformations. In *Proceedings of the 2007 ACM SIGGRAPH/Eurographics symposium on Computer animation* (2007), SCA '07. 3

[Bar84] BARR A. H.: Global and local deformations of solid primitives. In *Proceedings of the 11th annual conference on Computer graphics and interactive techniques* (1984), SIGGRAPH '84, pp. 21–30. 3

[BK03] BOTSCH M., KOBBELT L.: Multiresolution surface representation based on displacement volumes. *Comput. Graph. Forum 22*, 3 (2003), 483–492. 3

[CBC*07] CAPELL S., BURKHART M., CURLESS B., DUCHAMP T., POPOVIĆ Z.: Physically based rigging for deformable characters. *Graph. Models 69*, 1 (2007), 71–87. 3

[Chi95] CHIRIKJIAN G. S.: Closed-form primitives for generating locally volume preserving deformations. *Journal of Mechanical Design 117*, 3 (1995), 347–354. 3

[dC92] DO CARMO M. P.: *Riemannian Geometry*, 1st ed. Birkhäuser, 1992. 4

[DMSB99] DESBRUN M., MEYER M., SCHRÖDER P., BARR A. H.: Implicit fairing of irregular meshes using diffusion and curvature flow. In *Proceedings of the 26th annual conference on Computer graphics and interactive techniques* (1999), SIGGRAPH '99. 3

[FH03] FAROUKI R. T., HAN C. Y.: Rational approximation schemes for rotation-minimizing frames on pythagorean-hodograph curves. *Computer Aided Geometric Design 20*, 7 (2003), 435 – 454. 4

[Foo06] FOOTE R. L.: The volume swept out by a moving planar region. *Mathematics Magazine 79* (2006), 289–297. 7

[HML99] HIROTA G., MAHESHWARI R., LIN M. C.: Fast volume-preserving free form deformation using multi-level optimization. In *Proceedings of the fifth ACM symposium on Solid modeling and applications* (1999), SMA '99. 3

[HS97] HARRIS J. W., STOCKER H.: *The Handbook of Mathematics and Computational Science*, 1st ed. Springer-Verlag New York, Inc., Secaucus, NJ, USA, 1997. 2

[KCZO07] KAVAN L., COLLINS S., ZÁRA J., O'SULLIVAN C.: Skinning with dual quaternions. In *SI3D* (2007), pp. 39–46. 2, 3

[KLL*07] KIM B., LIU Y., LLAMAS I., JIAO X., ROSSIGNAC J.: Simulation of bubbles in foam with the volume control method. *ACM Trans. Graph. 26*, 3 (2007). 3

[LCF00] LEWIS J. P., CORDNER M., FONG N.: Pose space deformation: a unified approach to shape interpolation and skeleton-driven deformation. In *Proceedings of the 27th annual conference on Computer graphics and interactive techniques* (2000), SIGGRAPH '00. 1, 3

[Moo08] MOON H. P.: Equivolumetric offsets for 2d machining with constant material removal rate. *Computer Aided Geometric Design 25*, 6 (2008), 397 – 410. 3

[Moo09] MOON H. P.: Equivolumetric offset surfaces. *Computer Aided Geometric Design 26* (2009), 17 – 36. 3

[RHC08] ROHMER D., HAHMANN S., CANI M.-P.: Local volume preservation for skinned characters. *Comput. Graph. Forum 27*, 7 (2008), 1919–1927. 2, 3

[RHC09] ROHMER D., HAHMANN S., CANI M.-P.: Exact volume preserving skinning with shape control. In *Proceedings of the 2009 ACM SIGGRAPH/Eurographics Symposium on Computer Animation* (2009), SCA '09. 3

[RR87] ROSSIGNAC J., REQUICHA A.: Piecewise-circular curves for geometric modeling. *IBM Journal of Research and Development 3* (1987), 129–148. 4

[Sal99] SALOMON D.: *Computer Graphics and Geometric Modeling*, 1st ed. Springer-Verlag New York, Inc., 1999. 4

[Ste40] STEINER J.: über parallele flächen. *Monatsberichte der Akademie der Wissenschaft zu Berlin (Monthly Report of the Academy of Sciences, Berlin)* (1840), 114–118. 3

[STG*97] STORTI D. W., TURKIYYAH G. M., GANTER M. A., LIM C. T., STAL D. M.: Skeleton-based modeling operations on solids. In *Proceedings of the fourth ACM symposium on Solid modeling and applications* (1997), SMA '97. 3

[vFTS06] VON FUNCK W., THEISEL H., SEIDEL H.-P.: Vector field based shape deformations. In *ACM SIGGRAPH 2006 Papers* (2006), SIGGRAPH '06. 3

[ZR12] ZHUO W., ROSSIGNAC J.: Curvature-based offset distance: Implementations and applications. *Computers & Graphics 36*, 5 (2012), 445–454. 2, 3